Phase stability in a multistage Zeeman decelerator

Originally published in:
Physical Review A 82(4), https://doi.org/10.1103/PhysRevA.82.043428

The following article appeared in *Phys. Rev. A* **82**, 043428 (2010) and may be found at https://doi.org/10.1103/PhysRevA.82.043428.

Phase stability in a multistage Zeeman decelerator

A. W. Wiederkehr, S. D. Hogan, and F. Merkt

Laboratorium für Physikalische Chemie,

ETH Zürich, CH-8093, Switzerland

(Dated: September 22, 2010)

Abstract

The phase stability of a multistage Zeeman decelerator is analyzed by numerical particle-trajectory simulations and experimental measurements. A one-dimensional model of the phase stability in multistage Stark deceleration (Bethlem et al., Phys. Rev. Lett. **84**, 5744 (2000)) has been adapted to multistage Zeeman deceleration and compared with one- and three-dimensional particle-trajectory simulations, including the analysis of the effect of finite switch-on and -off times of the deceleration pulses. The comparison reveals that transverse effects in the decelerator lead to a considerable reduction of the phase-space acceptance at low values of the phase angle and an enhancement at high values. The optimal combinations of phase angles and currents with which a preset amount of kinetic energy can be removed from deuterium atoms in a pulsed supersonic beam using a 24-stage decelerator are determined by simulation. Quantitative analysis of the phase-space acceptance within a given volume reveals that for our decelerator (8 μs switch-off time) optimal conditions are achieved for values of the phase angle between 45° and 55°. This conclusion is examined and confirmed by experimental measurements. Alternative approaches to generate optimal deceleration pulse sequences, such as the implementation of evolutionary algorithms or the use of higher-order modes of the decelerator, are discussed.

PACS numbers: 37.10.Mn, 32.60.+i

I. INTRODUCTION

Over the last decade, substantial progress has been made in the development of techniques to produce cold samples of neutral atoms and molecules that cannot be laser cooled [1–4]. The need for such techniques is motivated by a wide range of applications in physics and chemistry such as precision measurements of fundamental frequency intervals [5], the study of collisions at very low temperatures [6] or exploiting a high degree of control over the kinetic energies of the colliding particles [7], the search for an electric dipole moment of the electron [8], or even measurements of the mass of the neutrino [9].

Several methods currently used to produce cold stationary samples of atoms and molecules are based on the deceleration of pulsed supersonic beams using time-dependent inhomogeneous electric (multistage Stark deceleration [10, 11] and Rydberg-Stark deceleration [12–15]) or magnetic (multistage Zeeman deceleration [16–19]) fields. Since these deceleration procedures rely on conservative forces, the achievable phase-space densities are limited by the phase-space characteristics of the sample prior to deceleration. Samples formed in pulsed supersonic expansions provide an attractive starting point for deceleration techniques thanks to their narrow longitudinal and transverse velocity spreads (corresponding to temperatures of ~ 1 K or less) combined with a high density of particles and a low internal (rovibrational) temperature. Optimal conditions can be achieved by lowering the initial longitudinal velocity of these beams using different carrier gases and cooling the gas sample prior to expansion.

The initial phase-space distribution of the sample can be preserved throughout the deceleration process by operating the decelerator in a so-called phase-stable manner. The concept of phase stability was first developed in the context of charged-particle acceleration [20, 21], but it also applies to the deceleration of neutral polar molecules in multistage Stark decelerators, as first demonstrated experimentally in the deceleration of CO molecules by Bethlem et al. [22] and, as explained in this article, to multistage Zeeman deceleration. Careful studies of the transverse phase-space stability in a Stark decelerator were essential to achieve efficient deceleration and simultaneously preserve a high phase-space density [23]. In particular, the conclusion was reached that the acceptance in phase space can be increased by exploiting higher-order modes of operation [24, 25]. An even larger phase-space acceptance can be reached using travelling electric potential wells, as first exploited in Rydberg-Stark deceleration [13, 14] and now also successfully used in the Stark deceleration of ground-state

molecules [26, 27].

In a recent work on the magnetic trapping of deuterium atoms after Zeeman deceleration, we found that consideration of the transverse motion is essential for the generation of dense, low-velocity samples in a multistage Zeeman decelerator [28]. Even though Zeeman decelerators share many common aspects with Stark decelerators, important differences exist in the mode of operation. These differences may prevent a direct transfer of the concepts developed and the knowledge gained in studies of phase stability in multistage Stark decelerators [23, 24, 29, 30] and justify a separate treatment of phase stability in multistage Zeeman decelerators.

Figure 1 schematically compares the standard modes of operation of Stark and Zeeman decelerators and reveals the main differences between the two types of decelerators. Firstly, Zeeman decelerators have a cylindrical symmetry along the beam axis, whereas the successive deceleration stages of Stark decelerators have their electrodes pointing alternatively along the x and the y axes of the decelerator. Quantitative differences may thus be expected in the transverse motion of the particles in the decelerator. Secondly, the Zeeman decelerator is operated by switching the current in the solenoids one after the other, whereas, in most Stark decelerators, the electric field configuration is switched between two configurations with interleaved sets of electrodes to which pulses of high and low potential are applied alternatively. The two different modes of operation result in a traveling effective saddle-shaped potential in a Zeeman decelerator and in a traveling array of effective potential wells in a Stark decelerator, so that differences are also expected for the longitudinal motion. Finally, the different time scales of the rise and fall times of the high current pulses applied to the solenoids of a Zeeman decelerator (typically $5-10$ μs) compared to those of the pulsed electric potentials applied to the electrodes of a Stark decelerator (typically $10-100$ ns) require a different treatment of phase angles.

In this article, we present a general analysis of the longitudinal and transverse motions in a multistage Zeeman decelerator, following the procedure established in Refs. [23, 29] for Stark deceleration. Although we present results on deuterium as illustration, this analysis is applicable to any paramagnetic atom or molecule. After presenting a one-dimensional model for the longitudinal phase-space stability, we then incorporate all relevant experimental constraints to establish, by simulation, a procedure to identify the optimal phase angle for efficient deceleration. The simulation results are then compared to experimental mea-

surements in which the phase angles and currents applied to the decelerator solenoids are systematically varied. We also discuss alternative approaches to the design of efficient pulse sequences in multistage Zeeman decelerators, making comparison with similar approaches developed in Stark-deceleration experiments [24, 31].

II. LONGITUDINAL MOTION AND TRANSVERSE EFFECTS IN A MULTISTAGE ZEEMAN DECELERATOR

A. A model for longitudinal phase stability

To develop a model describing the longitudinal phase stability in a multistage Zeeman decelerator we follow the ideas introduced for charged-particle accelerators [20, 21] and their adaptation to multistage Stark deceleration of polar molecules [22]. A multistage Zeeman decelerator consists of an array of solenoids along the axis of which a supersonic beam of paramagnetic species propagates (see Fig. 1). Each solenoid can be individually pulsed with a high current, resulting in a saddle-shaped potential for particles in low-field-seeking (lfs) quantum states (see bottom panel of Fig. 1). A particle in a lfs state decelerates as it moves into the solenoid because it gains potential energy. The deceleration process can be repeated stage by stage by rapidly switching off the current in the solenoid before the particle reaches the point of maximal magnetic field and switching on the current in the next solenoid. The amount of kinetic energy lost by a particle in a given deceleration stage depends on its position along the beam axis when the magnetic field is switched off. Because of the periodicity of the deceleration process, this position is given as a phase angle ϕ rather than a spatial coordinate. A phase angle of 0° corresponds to the middle point between two adjacent solenoids, and a phase angle of 90° to the center of the active solenoid where the magnetic field strength is maximal.

The calculation of a deceleration pulse sequence is carried out by defining an equilibrium phase angle ϕ_0 with respect to a synchronous particle moving along the decelerator axis with a given initial longitudinal velocity v_0. Each solenoid is switched off as soon as the synchronous particle reaches the equilibrium phase angle ϕ_0. Because of the spatial periodicity of the decelerator, the synchronous particle will always travel the same distance L, and thus lose the same amount of kinetic energy, during the time intervals separating the switch-off

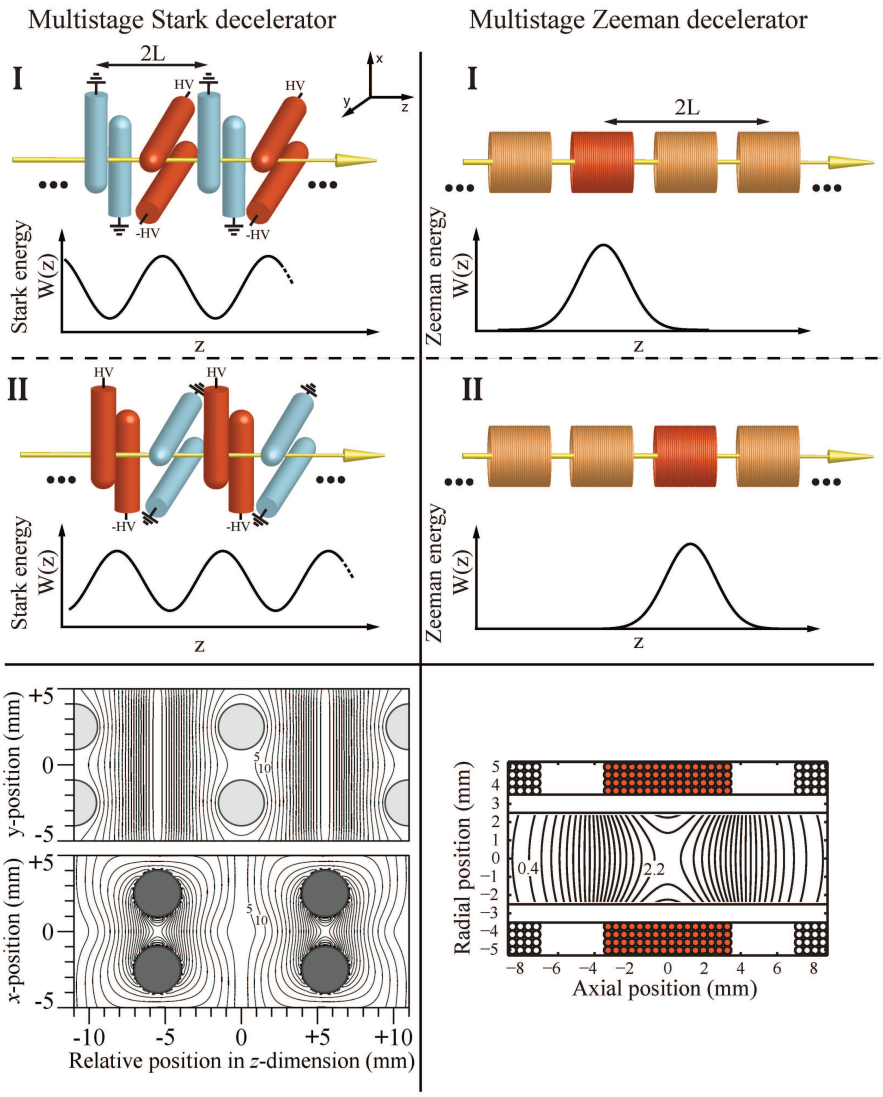

FIG. 1. Schematic comparison of the geometry and the standard mode of operation of multistage Stark (left-hand side) and multistage Zeeman (right-hand side) decelerators. The direction of propagation (z) of the supersonic beam is indicated by the arrows. The two panels (I, II) for each decelerator depict two subsequent configurations of a deceleration sequence. In a Stark decelerator, every second pair of electrodes are set to a high electric potential, leading to the sinusoidal form of the Stark energy $W(z)$ on axis of a polar molecule, as plotted below the set of electrodes. In a Zeeman decelerator, only one solenoid is switched on at a time, giving rise to a single-peaked Zeeman energy $W(z)$. The bottom panels display the relevant field distributions. The electric field distribution is depicted for a Stark decelerator with its electodes pulsed as in configuration I. The contours of constant electric (magnetic) field strength are drawn in steps of 5 kV/cm (0.1 T).

times of adjacent solenoids, assuming that the currents are identical and can be switched on and off instantaneously. A particle initially at the same position as the synchronous particle, but having a slightly higher (lower) velocity, will have moved further (less far) into the solenoid than the synchronous particle by the time the current is switched off, resulting in a higher (lower) phase angle ϕ and more (less) deceleration. Over several deceleration stages this particle will gain (lose) phase angle relative to the synchronous particle until its velocity is reduced (increased) to v_0. After this time, the particle starts losing (gaining) phase angle and velocity relative to the synchronous particle until it reaches the same phase angle but with a negative (positive) relative velocity. An oscillatory motion around the synchronous particle results.

To quantitatively model this behavior, we first assume an instantaneous switch on and switch off of the current in the solenoids. The influence of the finite switch-on and -off times that are unavoidable in multistage Zeeman deceleration will then be analyzed by comparison of the model predictions with the results of particle-trajectory simulations. The kinetic energy $\Delta T(\phi_0)$ that is lost by the synchronous particle per stage is equal to the potential energy difference $W(\phi_0) - W(\phi_0 - \pi)$. In contrast to a Stark decelerator, where $W(\phi)$ can be expressed to first approximation by a sinusoidal function, only one solenoid is active at a given time in a Zeeman decelerator generating a single-peaked potential-energy function (see Fig. 1). For values of the equilibrium phase angle $\phi_0 - \pi$ smaller than 0, the potential energy can be neglected to good approximation, so that $\Delta T(\phi_0) \approx W(\phi_0)$. Assuming that the velocity change per deceleration stage is small compared to v_0, the loss in kinetic energy can be regarded as originating from a continuously acting average force, $\bar{F} = -W(\phi_0)/L$.

Nonsynchronous particles can be described by their instantaneous relative phase, $\Delta\phi(t) = \phi(t) - \phi_0$, and velocity $\Delta v(t) = v(t) - v_0$, with respect to the synchronous particle. As long as $\Delta v \ll v_0$, the average force acting on a nonsynchronous particle is $\bar{F}(\phi_0 + \Delta\phi) \approx -W(\phi_0 + \Delta\phi)/L$, so that its motion relative to the synchronous particle is described to good approximation by:

$$\frac{mL}{\pi}\frac{\mathrm{d}^2\Delta\phi}{\mathrm{d}t^2} + \frac{1}{L}\left(W(\phi_0 + \Delta\phi) - W(\phi_0)\right) = 0, \tag{1}$$

where m is the mass of the particle. In the remainder of this article, we present results for deuterium atoms, for simulations as well as for experimental investigations. However, the

general conclusions are equally well applicable to any other paramagnetic species by making the corresponding adjustments of m and W in Eq. (1).

To find the longitudinal phase-space acceptance of the Zeeman decelerator, Eq. (1) is integrated numerically assuming that the Zeeman energy $W(\phi)$ of a deuterium atom in the field of a solenoid is well approximated by a Gaussian function

$$W(z) = a\mathrm{e}^{-\frac{(z-b)^2}{2c^2}}. \tag{2}$$

The parameter values $a = 1$ cm^{-1}, $b = 5.50$ mm and $c = 3.76$ mm accurately describe $W(z)$ for the solenoids of our decelerator (inner diameter 7 mm; 64 windings; 4 layers; wire diameter 400 μm; current 300 A; distance between the centers of adjacent solenoids $L = 11$ mm, see Ref. [28]). Numerical integration leads to the set of phase-space diagrams obtained for equilibrium phase angles ϕ_0 varying in the range from 0 to $\pi/3$ depicted in Fig. 2. The bold line in each plot, called separatrix, represents the boundary between the region in phase space where the particles undergo stable phase-space rotations around the synchronous particle and the region where the trajectories are unstable. The phase-space area inside the separatrix decreases with increasing value of ϕ_0 because of the decrease of the potential energy difference $W(\pi/2) - W(\phi_0)$. The energy loss per stage, however, increases with increasing ϕ_0, resulting in a trade off between large acceptance and efficient deceleration.

The phase-space diagrams presented in Fig. 2 are similar in form and size to those obtained for Stark decelerators in Ref. [29]. The only evident differences, which originate from the nonperiodic shape of $W(z)$ (compare the plots of Stark and Zeeman potential energy in Fig. 1), are (i) that the $\phi_0 = 0$ separatrix is not symmetric with respect to the inversion through the point (ϕ_0, $\Delta v_0 = 0$) as in a Stark decelerator, and (ii) that there is only one area of phase stability in the case of a Zeeman decelerator but an array of such areas in the case of a Stark decelerator.

B. Particle-trajectory simulations and transverse phase stability in multistage Zeeman deceleration

The one-dimensional model presented in the previous subsection offers a useful starting point to estimate the deceleration pulse sequences and to discuss the general aspects of

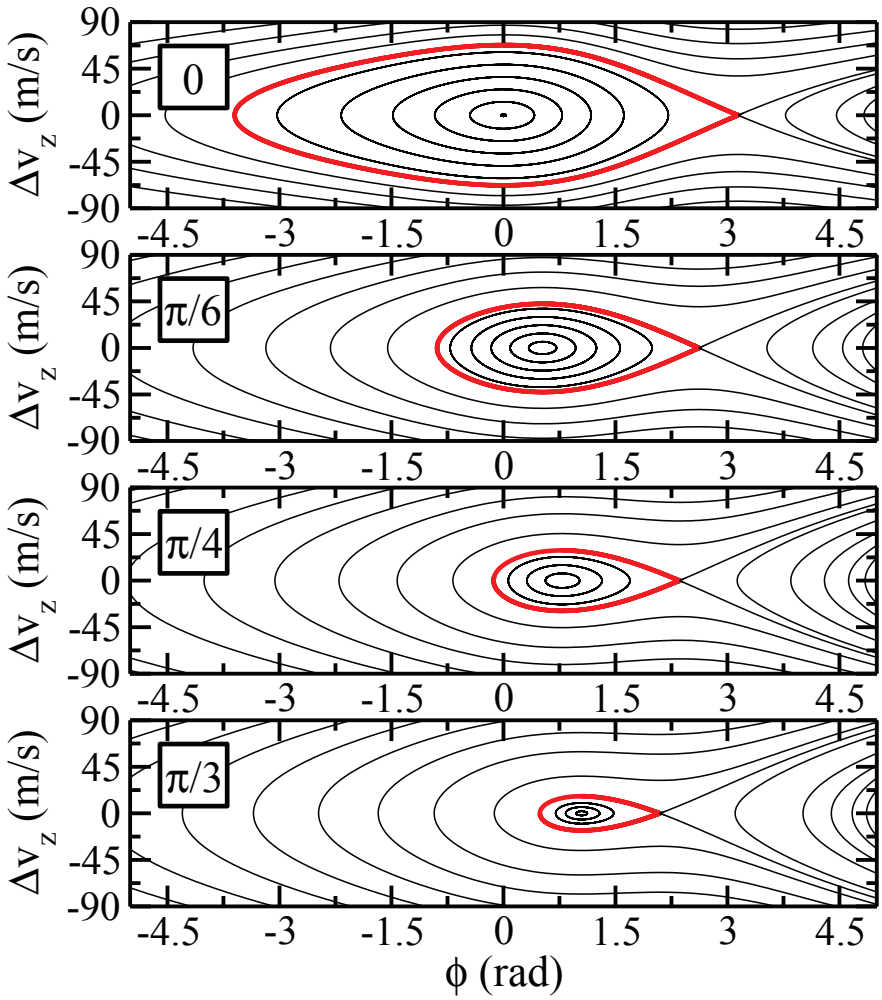

FIG. 2. Phase-space diagram for different values of the equilibrium phase angle ϕ_0 (denoted in the inset of each graph) plotted as a function of the phase angle ϕ and the relative velocity Δv_z with respect to the synchronous particle. The curves result from numerical integration of Eq. (1) using different initial conditions and parameters as described in the text. In each graph, the separatrix marking the boundary between the stable and the unstable regions in phase space is drawn as bold line.

the deceleration behavior. Its approximate nature and the assumptions on which it relies, however, limit its predictive power. Particle-trajectory simulations, though computationally much more demanding, are necessary to assess its limitations and to gain a quantitatively satisfactory understanding of the operational characteristics of a multistage Zeeman decelerator. A three-step procedure was followed to quantify the phase-space acceptance of our multistage Zeeman decelerator by particle-trajectory simulations. In a first step, one-

dimensional particle-trajectory simulations were carried out to investigate the effects of the finite length of the decelerator and to go beyond the approximation of neglecting the condition of constant velocity upon which Eq. (1) is based. In the second step, three-dimensional particle-trajectory simulations were performed to quantify the effects of the transverse motion on the phase-space acceptance of the decelerator, assuming idealized magnetic field pulses of infinitely short rise and fall times. In the last step, the effects of the finite rise time of the magnetic field pulses (~ 8 μs in our current decelerator [28]), which are significant in multistage Zeeman deceleration (the rise times of electric field pulses in Stark decelerators are much shorter (typically less than 100 ns), and their effects can be neglected [10]), were investigated by three-dimensional particle-trajectory simulations.

The computations relied on the use of the magnetic field distributions corresponding to the solenoids employed in our recent experiments [28]. Initial sets of particles uniformly distributed in a phase-space volume larger than the anticipated acceptance volume of the decelerator were used, and the phase-space acceptance of the decelerator was determined for specific values of equilibrium phase angle, number of stages and current by drawing points in the phase-space diagrams corresponding to the final positions and velocities of all particles having undergone deceleration. For the sake of comparison of the results of the different simulations, the length of the decelerator and the initial velocity of the synchronous particle were chosen such that, in all cases, its final velocity was 300 m/s and the time taken for the deceleration process was ~ 1.5 ms.

Each of the three steps outlined above provides specific insights, and the results of the corresponding simulations, presented in the three columns of Fig. 3, are now discussed in turn.

1. One-dimensional particle-trajectory simulations

The results of the one-dimensional particle-trajectory simulations are depicted in the left column of Fig. 3. For each simulation, the trajectories of $2.5 \cdot 10^5$ deuterium atoms, uniformly distributed in phase space, were computed, and for each trajectory the position (phase angle) and velocity of the particles were sampled immediately after the switch off of the last solenoid and plotted in relative coordinates with respect to the synchronous particle. Simulations were performed for four equilibrium phase angles $\phi_0 = 0$, $\pi/6$, $\pi/4$, $\pi/3$, and,

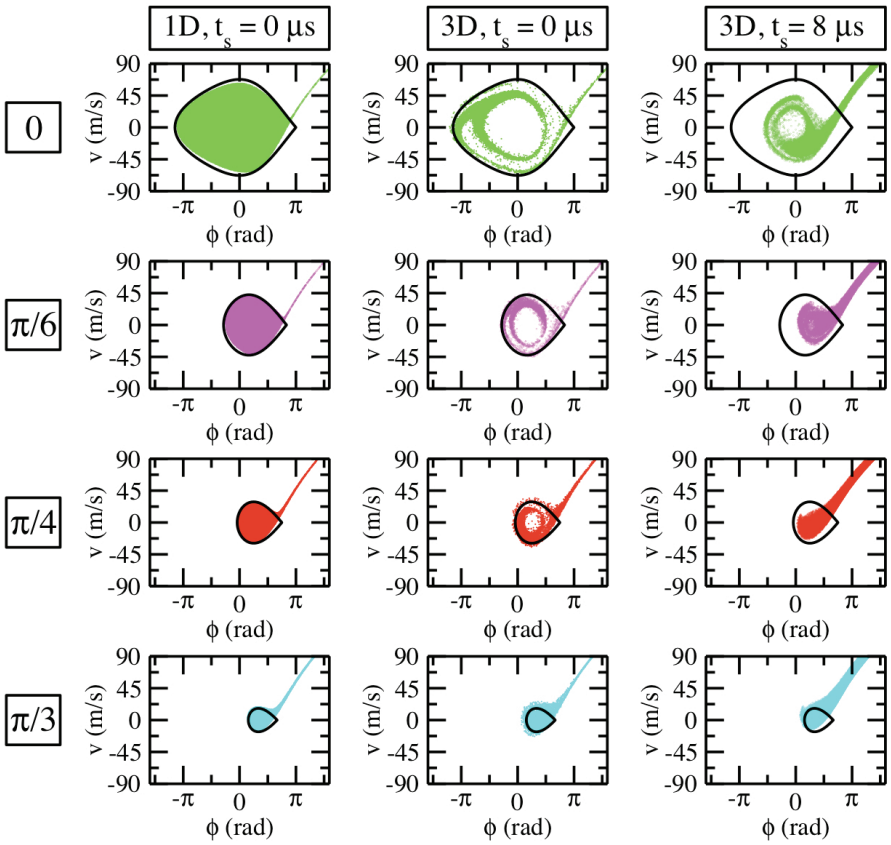

FIG. 3. Comparison of the one-dimensional phase-stability model with particle-trajectory simulations for selected values of ϕ_0 (increasing from top to bottom). Left and middle columns: one- and three-dimensional particle-trajectory simulations assuming instantaneous switch off of the current (i.e., $t_s = 0$), respectively. Right column: Three-dimensional particle-trajectory simulations taking into account the $t_s = 8$ μs switch-off time of the currents. The bold line in each graph shows the separatrix derived using Eq. (1).

for comparison, the separatrices obtained from Eq. (1) are also drawn in the phase-space diagrams. The corresponding number of stages decreases from 80 ($v_{\text{in}} = 660$ m/s) for $\phi_0 = 0$ to 56 ($v_{\text{in}} = 820$ m/s) for $\phi_0 = \pi/3$ to account for the fact that the deceleration achieved per stage increases with the value of the equilibrium phase angle. In a multistage Stark decelerator, an equilibrium phase angle of $\phi_0 = 0$ results in no deceleration, but only guiding of the beam, because of the spatial periodicity of the Stark energy (see Fig. 1). In a multistage Zeeman decelerator, the Zeeman energy and its gradient are nonzero at the position $\phi_0 = 0$, so that a weak deceleration results.

The following conclusions can be drawn from the phase-space diagrams:

(i) The separatrix calculated from Eq. (1) corresponds almost exactly to the boundary of the phase-space distribution of the particles transmitted (and decelerated) by the Zeeman decelerator for all four equilibrium phase angles. Moreover, the bunch of transmitted particles forms a homogeneous (structureless) distribution inside the separatrix. Eq. (1), therefore, represents an adequate description of the one-dimensional particle-trajectory simulations.

(ii) A small group of transmitted atoms lies outside the area enclosed by the separatrix and forms a band extending toward the high-velocity and high-phase-angle corner of the phase-space diagrams. The thickness of this band and the number of particle trajectories that contribute to it increase with increasing value of ϕ_0, and decreasing number of deceleration stages. This deviation from the behavior predicted by Eq. (1) was found to be a consequence of the finite length of the decelerator by carrying out simulations for decelerators of different lengths. This aspect is discussed further in Subsection II B 3.

(iii) The phase-space distribution of the transmitted particles is characterized by a slight counter-clockwise rotation with respect to the separatrix. Analysis of the trajectories enables one to attribute this effect to the fact that the energy removed by each deceleration stage is not entirely negligible compared to the kinetic energy, as was assumed in the derivation of Eq. (1).

Whereas the agreement between the longitudinal phase-space acceptance model and the results of one-dimensional particle-trajectory simulations can be regarded as excellent, it is nevertheless important, for the following discussion of three-dimensional particle-trajectory simulations, to remember that the sources of deviations mentioned under points (ii) and (iii) above are purely longitudinal effects and cannot be attributed to the transverse motion.

2. Three-dimensional particle-trajectory simulations and transverse motion in a multistage Zeeman decelerator

To obtain the results of the three-dimensional particle-trajectory simulations depicted in the middle column of Fig. 3, the initial distribution of the particles was modified to account for the transverse dimensions (x,y). The longitudinal components were distributed as in the one-dimensional simulations. Uniform initial transverse position and velocity distributions were chosen, and the size of the phase-space volume was increased until the number of particles transmitted by the decelerator had converged ($|v_x|, |v_y| \leq 30$ m/s; $|x|, |y| \leq$

2.5 mm). The particle-trajectory simulations were performed with exactly the same pulse sequences as in the one-dimensional case, but with an increased number of particles (10^6).

Comparing the results of the one- and three-dimensional particle-trajectory simulations enables one to quantify changes in the longitudinal phase-space acceptance resulting from transverse forces. At low values of ϕ_0, no stable particle trajectories are observed in a circular phase-space area centered around the synchronous particle and in an almost closed ring immediately inside the separatrix. Transverse effects thus significantly reduce the phase-space acceptance of the decelerator. However, the size of the nonaccepted areas rapidly decreases at increasing values of the phase angle. The simulations also reveal that the separatrix obtained from the one-dimensional model (Eq.(1)) still represents an approximate boundary of the longitudinal phase-space acceptance of the decelerator. At values of the equilibrium phase angle ϕ_0 beyond $\pi/4$, the longitudinal acceptance area of the decelerator even becomes larger than the area enclosed by the separatrix.

The area in the middle of the separatrix that is not accepted by the decelerator and its decrease in size with increasing equilibrium phase angle ϕ_0 was found, by analyzing the trajectories of the nonaccepted particles, to be a result of the convex shape of the transverse magnetic field distribution outside the solenoid (see Fig. 1), which results in a transverse defocusing force. For the particles to remain within the physical boundaries of the decelerator, this defocusing force needs to be compensated, over a full period of oscillation around the position of the synchronous particle, by the (stronger) focusing forces which result from the concave magnetic field distribution inside the active solenoid. At low values of the equilibrium phase-angle ϕ_0, the particles moving off-axis and located in longitudinal phase space close to the synchronous particle will hardly experience any focusing forces. At $\phi_0 = 0$, for instance, a particle with the same longitudinal velocity as the synchronous particle, but additional off-axis velocity components, needs a relative difference in phase angle of $\sim \pi/2$ to experience enough focusing forces to be accepted by the decelerator (see top panel of the middle row of Fig. 3). The synchronous particle moves further into the solenoid with increasing equilibrium phase angle ϕ_0. Consequently, the minimal phase-angle difference a particle must have with respect to the synchronous particle to balance the transverse forces decreases, resulting in a smaller size of the longitudinal phase-space area around the synchronous particle that is not accepted by the decelerator. At phase angles beyond $\pi/4$, the nonaccepted area inside the separatrix completely vanishes, and all particles

close to the synchronous particle are accepted by the decelerator.

In Stark decelerators, one also observes a reduced acceptance around the synchronous particle at low equilibrium phase angles (see Fig. 3 of Ref. [23]), because the transverse forces are insufficient to confine the transverse motion of the particles with phase angles similar to that of the synchronous particle and significant transverse velocities. This reduction, however, is not as large as for Zeeman decelerators, because of the reduced effects of transverse defocusing forces in Stark decelerators (see bottom panels of Fig. 1).

At low equilibrium phase angles, the phase-space acceptance is not only reduced in the center of the phase-space diagrams (see Fig. 3), but also close to the separatrix. The simulations reveal that particles in these regions oscillate around the synchronous particles with a high-phase-angle turning point close to the center of the active solenoid, where the transverse forces are strongest. The resulting gain in transverse velocity is so large that it cannot be compensated any more. The simulations show that these particles eventually collide with the walls of the glass tube around which the solenoids are wound.

In Stark decelerators, unstable regions close to the separatrix, often referred to as halos [23] because of their ring structure, are observed as well. The depletion of these regions is caused by parametric amplification of the transverse oscillations of particles having phase-space coordinates such that the transverse and the longitudinal oscillation frequencies are similar. The strong coupling of the transverse and longitudinal motion in Stark deceleration arises because the transverse focusing forces, after decreasing from $\phi = \pi/2$ to $\phi = 0$, increase again from $\phi = 0$ to $\phi = -\pi/2$ as a result of the periodicity of the Stark energy $W(\phi)$.

In the three-dimensional particle-trajectory simulations depicted in Fig. 3, stable trajectories are observed again for particles with even larger differences in phase angle to the synchronous particle than the unstable trajectories discussed above. These trajectories belong to particles which, during their longitudinal oscillations around the synchronous particle, reach phase angles close to the exit of the active solenoid. The overall effect is a compensation of the focusing force during an oscillation period that is such that these particles enter the regions of low transverse forces with a moderate displacement from the beam axis and vanishing transverse velocity components, leading to stable trajectories.

At values of the equilibrium phase angle higher than $\pi/4$, the separatrix covers a region of phase angles where the transverse field distributions in Stark decelerators, in the direction

perpendicular to the plane spanned by the active rods, and in Zeeman decelerators are qualitatively similar, so that the nonperiodicity of the Zeeman energy does not play a significant role. The enhanced phase-space acceptance of Zeeman decelerators observed at these values of the equilibrium phase angle (see middle column Fig. 3) is therefore analogous to that observed in Stark decelerators (see Ref. [23]): Because of the convex (concave) magnetic field curvature outside (inside) the solenoid, particles with off-axis velocity components and positions experience a larger change in Zeeman energy between two successive switch-off times of the solenoids than the synchronous particle. The pulse sequence calculated for the (on-axis) synchronous particle is therefore optimal for off-axis particles having a lower equilibrium phase angle, which results in a higher overall longitudinal acceptance.

3. Effects of the finite rise and fall times of the currents in the solenoids

The right column of Fig. 3 shows the results of three-dimensional particle-trajectory simulations including a finite switch-off (switch-on) time $t_s = 8$ μs of the current in the solenoids. To be consistent with earlier publications [17, 28, 32], we define the (nominal) phase angle ϕ_0 as the position of the synchronous particle at the time the current switch-off process is initiated. The pulse sequences for the same initial and the same final velocities of the synchronous particle as used in the subsections II B 1 and II B 2 had to be modified to account for the fact that the particles continue to experience a magnetic field gradient, and decelerate during the current switch-off process. This effect causes the particle to experience a higher (effective) phase angle ϕ_{eff} and to loose more kinetic energy. Consequently, fewer stages are needed to remove the same amount of kinetic energy for a given equilibrium phase angle ϕ_0, resulting in a shorter time spent by the particles in the decelerator. Comparing the simulations including the finite switch-off times with those that neglect it (middle column in Fig. 3) leads to the following conclusions: (i) The band of particles outside the separatrix extending to the high-velocity, high-phase-angle corner of the diagrams is thicker. As explained in subsection II B 1, this feature depends on the time the particles spend in the decelerator and can therefore be attributed to the reduced number of deceleration stages compared to the simulations with $t_s = 0$ μs. (ii) The decelerated particles are confined in a smaller area than that given by the separatrix (at least for the three lower phase angles), and (iii) the area corresponding to particles with transversely unstable trajectories near the

center of the phase-space diagram is smaller, or has even vanished. The second and third features arise from the finite switch-off time: The synchronous particle continues moving into the solenoid while its current is switched off, resulting in a higher effective phase angle $\phi_{eff} > \phi_0$. Consequently, the phase-stable area determined for $\phi_0 = 0$ in simulations including finite switch-off times is better described by the separatrix corresponding to $\phi_0 = \pi/6$ than by the one corresponding to $\phi_0 = 0$. The higher effective phase angle resulting from the finite switch-off time also explains the more rapid decrease of the areas corresponding to unstable trajectories of the decelerated particles. Indeed, a particle that is located outside the solenoid at the time the solenoid is switched off can still experience a net focusing force in the transverse direction if it gets far enough into the solenoid during the switch-off process.

From the comparison of the last two columns of Fig. 3, we conclude that an operation of the decelerator at a value of ϕ_0 between $\pi/6$ and $\pi/3$ is desirable to reach an optimal compromise between efficient deceleration and high phase-space acceptance. In Section III, we will specify this optimal range of operation more precisely by comparison with experiments and simulations that model the complete geometry of our own experimental setup.

4. Higher-order modes of operation of a multistage decelerator

In multistage Stark deceleration, the higher-order $s = 3$ mode of operation was demonstrated to have a better acceptance than the constant-phase-angle ($s = 1$) mode of operation [25]. In the $s = 3$ mode, the deceleration is achieved by operating only every third stage as a deceleration stage, the intermediate stages being used to provide additional transverse focusing forces during the passage of the decelerated bunch, and so increase the phase-space acceptance. The $s = 3$ mode of operation of Stark decelerators can be analytically calculated by taking into account the higher-order Fourier coefficients of the Stark energy $W(z)$ (see Figure 1) in the model of its longitudinal phase-space acceptance (see Ref. [24] for a detailed discussion).

Because of the nonperiodicity of the Zeeman energy, an adaptation of the $s = 3$ mode of operation to Zeeman deceleration does not appear justified at first sight. Nevertheless, the concept of the $s = 3$ mode, which leads to an effective decoupling of the transverse and the longitudinal motions by performing longitudinal and transverse focusing operations using distinct stages, might also be implemented in multistage Zeeman decelerators. Two

possible strategies to mimic, in a Zeeman decelerator, the $s = 3$ mode of operation of a Stark decelerator are illustrated in Fig. 4. In the first strategy, the deceleration stages are divided into sets of three adjacent solenoids, the first and third solenoids of each set being connected in series and switched off simultaneously when the synchronous particle reaches a phase-angle $\phi_0 = 0$ with respect to the third solenoid. The second solenoid remains inactive throughout (i.e., it is removed) so that the magnetic field experienced by the synchronous particle during the deceleration process corresponds to that depicted in the bottom left panel of the figure. This distribution is almost identical to the corresponding electric field distribution experienced by the synchronous particle in a Stark decelerator operated in the $s = 3$ mode (compare with Fig. 2 of Ref. [25]). The deceleration procedure is carried out by repeating the deceleration steps involving three solenoids as the particles move through the decelerator. The second strategy, with which a very similar distribution of Zeeman energy can be realized for the synchronous particle (see bottom right panel in Fig. 4), consists of increasing the distance between adjacent solenoids and pulsing only every second solenoid at ϕ_0 while maintaining the current in the other solenoid on during the passage of the atom bunch.

Three-dimensional particle-trajectory simulations were carried out to validate these strategies. In the simulations, a current of 300 A was assumed, and the pulse sequences were designed to decelerate the D atoms from 660 m/s to 300 m/s using 240 (including the inactive solenoids) and 164 solenoids for the first and second strategy, respectively. The resulting phase-space acceptance diagrams are depicted in the upper panels of Fig. 4 and reveal two of the essential characteristic features of the $s = 3$ operation mode of Stark decelerators: Firstly, phase-stable operation is achieved both in the longitudinal and transverse dimensions, as indicated by the homogeneous areas of the diagrams around the position of the synchronous particles. Secondly, the longitudinal phase-space acceptance is reduced because the homogeneous area is smaller than the area inside the separatrix. Both strategies achieve the same decoupling of longitudinal and transverse forces in Zeeman deceleration as the $s = 3$ mode of Stark decelerators. Their implementation necessitates twice as many solenoids and larger decelerators, but would offer enhanced flexibility. In the implementation of these strategies in the particle-trajectory simulations, we used solenoids identical to those used in the simulations and experiments described in other parts of this article. For such solenoids, the first strategy leads to a larger phase-space acceptance (compare the

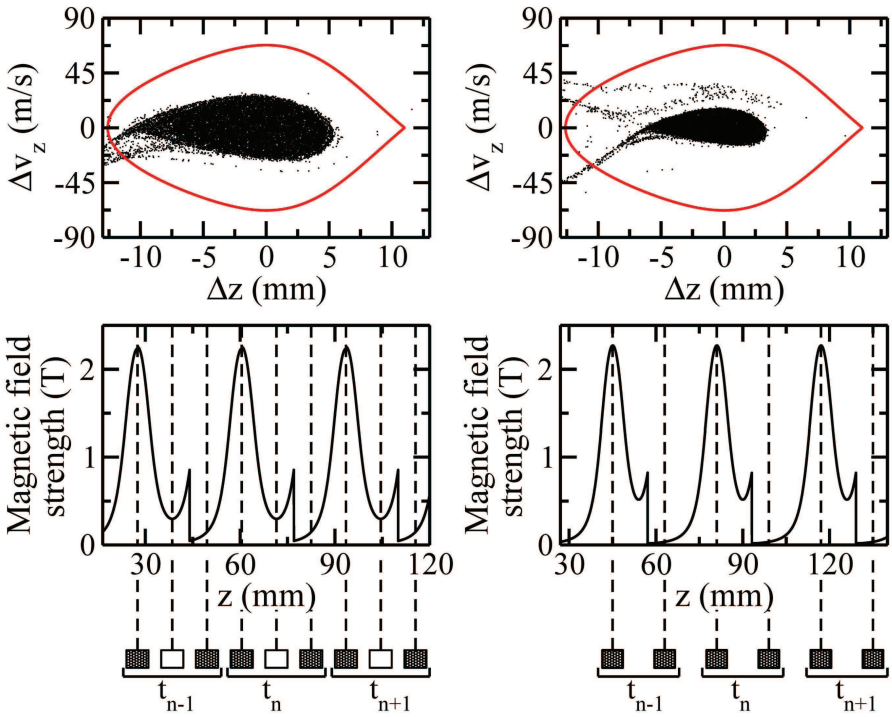

FIG. 4. Particle-trajectory simulations for the operation of a Zeeman decelerator mimicking the $s = 3$ mode of Stark decelerators. The left- and right-hand-side panels show the results for the two strategies discussed in the text. The top panels depict the results of three-dimensional particle-trajectory simulations overlaid with the separatrix obtained for the $\phi_0 = 0$ equilibrium-phase-angle mode of operation. The middle panels display the corresponding magnetic field strength as a function of the longitudinal position of the synchronous particle, displaying only a restricted number of stages for clarity. The bottom panel schematically depicts the arrangement of the solenoids.

upper panels of Fig. 4).

One should note that both modes of operation would be better described as being similar to $s = 2$ modes of operation. The reason why no $s = 2$ modes of operation is possible in a Stark decelerator is because subsequent stages have their electrodes pointing alternatively in the x and y directions. An $s = 2$ mode would therefore only refocus the particle bunches in one of two transverse dimensions. The cylindrical symmetry of Zeeman decelerators, however, makes $s = 2$ modes possible.

III. OPTIMIZED PULSE SEQUENCES IN MULTISTAGE ZEEMAN DECELERATION: COMPARISON WITH EXPERIMENT AND CONCLUSIONS.

In multistage deceleration, be it Stark or Zeeman, samples of cold molecules are decelerated to a given desired final velocity, usually chosen for a given experiment (e.g., magnetic trapping, electrostatic trapping, collision studies with slow beams of molecules of well-defined velocity, . . .). The final velocity determines the number of deceleration stages, the length of the decelerator and the deceleration temporal pulse sequence. In the case of D, velocities below 90 m/s are useful for trapping experiments, and velocities above 90 m/s are also useful in collision experiments. In this section, we seek to establish optimal strategies to generate samples moving at a given final velocity.

The most widespread mode of operation of multistage Stark decelerators is one in which the electric field pulses are switched on and off at constant phase angles. This mode of operation enables phase-stable deceleration both in the longitudinal and transverse dimensions [10, 23]. The finite rise and fall times of the magnetic field pulses in multistage Zeeman decelerators pose problems in the determination and implementation of pulse sequences operated at constant phase angles, because the nominal phase angle, which corresponds to the switch-off time of the solenoids, differs from the effective phase angle, which itself depends on the instantaneous velocity of the synchronous particle [28].

In Zeeman deceleration, two limiting operation modes can be envisaged to approximate the constant-phase-angle operation mode of Stark deceleration: a mode in which the deceleration process is carried out at constant *nominal* phase angle, and one in which the energy removal per stage is constant. In the former mode of operation, the *equilibrium* phase angle ϕ_0 is defined at the time when the current switch-off process is initiated, so that the amount of kinetic energy removed from the synchronous particle decreases from one stage to the next. In the latter mode of operation, the kinetic energy removed by the deceleration stages remains constant throughout the deceleration process, and the nominal phase angle increases from one stage to the next. This mode of constant energy removal per stage for the synchronous particle corresponds more closely to the standard mode of operation of deceleration with zero switch-off times. Both modes of operation become identical in the low-velocity limit, for which the distance travelled by the synchronous particle during the switch-off process is negligible. In the present section, we first present a characterization

of these two modes of operation by simulations in the case of the deceleration of D atoms with our 24-stage decelerator, and then compare the particle-trajectory simulations with experimental results. Finally, we briefly discuss other operational modes with which cold dense samples can be generated by multistage Zeeman deceleration.

A. Constant-phase-angle modes of operation

The multistage Zeeman decelerator employed in our studies is modular and consists of sections of 12 solenoids each, separated by a pumping region equipped with two coaxial collimation solenoids (see Fig. 1 of Ref. [28]). Current pulses of up to 300 A with rise and fall times of 8 μs can be applied separately to each solenoid. The collimation solenoids located between the different sections are connected in series and are held at a current of 240 A during the passage of the atomic beam. The supersonic beam of D atoms has a mean initial velocity of 475 m/s, with full widths at half maximum of 80 m/s and 4 m/s in the longitudinal and transverse dimensions, respectively.

To compare the constant-nominal-phase-angle and constant-energy-removal operational modes of the decelerator, we examined sequences with which the initial velocity is reduced from 475 m/s to final velocities v_f in the range between 90 and 180 m/s. Two sections (i.e., 24 deceleration solenoids) are sufficient to achieve the corresponding removal of kinetic energy. The general behavior turned out to be independent of the final velocity, so that only results for $v_f = 90$ m/s and 150 m/s are presented in detail.

Fig. 5 summarizes the results of a set of simulations of the deceleration of the D atom beam to 90 m/s using the constant-nominal-phase-angle mode of the decelerator. The simulations were carried out for several nominal phase angles between 18° and 60°. Because of the fixed length of the decelerator and the preset initial and final velocities, the current had to be adapted to the values of the selected nominal phase angle, high (low) currents being necessary in combination with low (high) phase angles. The left-hand-side panel of the figure shows the computed time-of-flight (TOF) distributions determined at the exit of the last solenoid of the decelerator. The different traces were shifted along the vertical axis for clarity, and the dashed horizontal lines indicate the relevant zero level of the intensity scale. As explained in Ref. [28], the TOF distributions consist of several sharp peaks at early times (< 1.5 ms), which arise from atoms that are guided through the decelerator

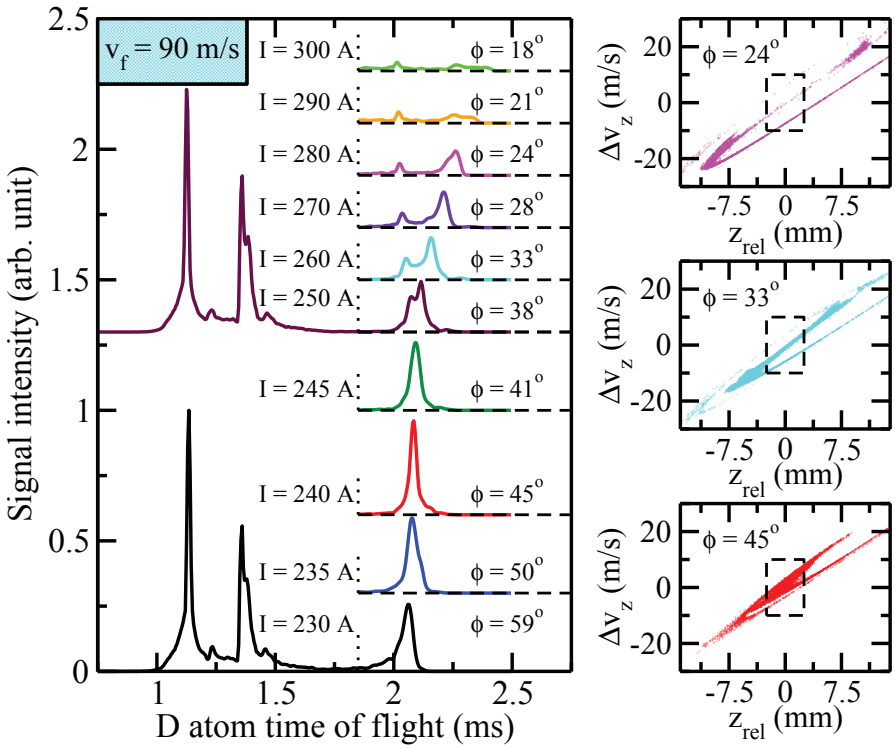

FIG. 5. Simulations of the deceleration of deuterium atoms with identical initial phase-space distribution to a given final velocity of 90 m/s using the constant-nominal-phase-angle operation mode of a 24-stage Zeeman decelerator. The left-hand-side panel depicts the detected time-of-flight distribution of the deuterium atoms for several combinations of phase angles ϕ_0 and currents I. Right-hand side: Phase-space distributions at the end of the decelerator for phase angles ϕ_0 of 24°, 33° and 45°. The dashed rectangles indicate the areas in longitudinal phase space for which magnetic trapping has been achieved.

without experiencing significant deceleration. The TOF distributions of these guided atoms are insensitive to the phase-angle/current combination and remain almost identical for all traces.

The decelerated bunches of atoms with a final velocity of 90 m/s correspond to the TOF peaks located just after 2 ms. At high nominal phase angles ϕ_0, this peak is sharp and it has maximal intensity for the 45°/235 A combination. At phase angles below 40°, the decelerated atoms form a bimodal TOF distribution, and the distance between the two components increases rapidly with decreasing phase angle. The phase-space distributions of the decelerated particles presented in the three panels on the right-hand side of the

figure provide additional information. The dashed frames at the center of these diagrams highlight the regions of phase space in the immediate vicinity of the synchronous particle and correspond to regions of the initial phase-space distributions for which magnetic trapping has been achieved [28]. The phase-space diagram obtained for $\phi_0 = 45°$ reveals a strong accumulation of particles around the synchronous particle, as expected for an efficient and phase-stable deceleration process. At phase angles of 33° and 24°, the region closest to the synchronous particle is depleted, and the diagrams indicate that the deceleration process is optimal only for two groups of D atoms with initial velocities differing by 5 m/s and 10 m/s, respectively. The depletion of the phase-space diagram is reminiscent of the discussion, in section II B, of transverse losses in the decelerator, which effectively prevent the observation of particles with longitudinal velocities similar to that of the synchronous particle at low equilibrium phase angles (see left-hand side of Fig. 3). The overall conclusions derived from Fig. 3 thus also appear to hold for the relatively short decelerator and the slightly modified geometry considered here.

Fig. 6 presents particle-trajectory simulations obtained with the constant-energy-removal mode of the decelerator, for a final velocity of 90 m/s. In the first deceleration stages, the effective phase angle is significantly larger than the nominal one, so that the value of the nominal phase angle leading to a preset loss of kinetic energy increases from one solenoid to the next. This in turn poses a limitation on the current, which cannot be reduced below 250 A. As in the case of Fig. 5, high currents correspond to low phase angles and vice versa. At high currents, a constant removal of energy implies a very low nominal phase angle and a low effective phase angle, so that the defocusing effects of the convex regions of the magnetic field distribution are dominant. The general aspects of the TOF distributions displayed in the left-hand side of the figure and of the phase-space diagrams presented in its right-hand side are qualitatively similar to those obtained with the constant-nominal-phase-angle mode of operation. It thus appears that both modes of operation lead to phase-stable deceleration both in the longitudinal and transverse dimensions, provided that the phase angle is large enough. That this would be the case was not obvious to us at the beginning of this investigation.

The results of all particle-trajectory simulations are summarized in Fig. 7 which displays, as a function of the current, the normalized phase-space densities obtained with both modes of operation for four values of the final velocity, the squares and circles corresponding to

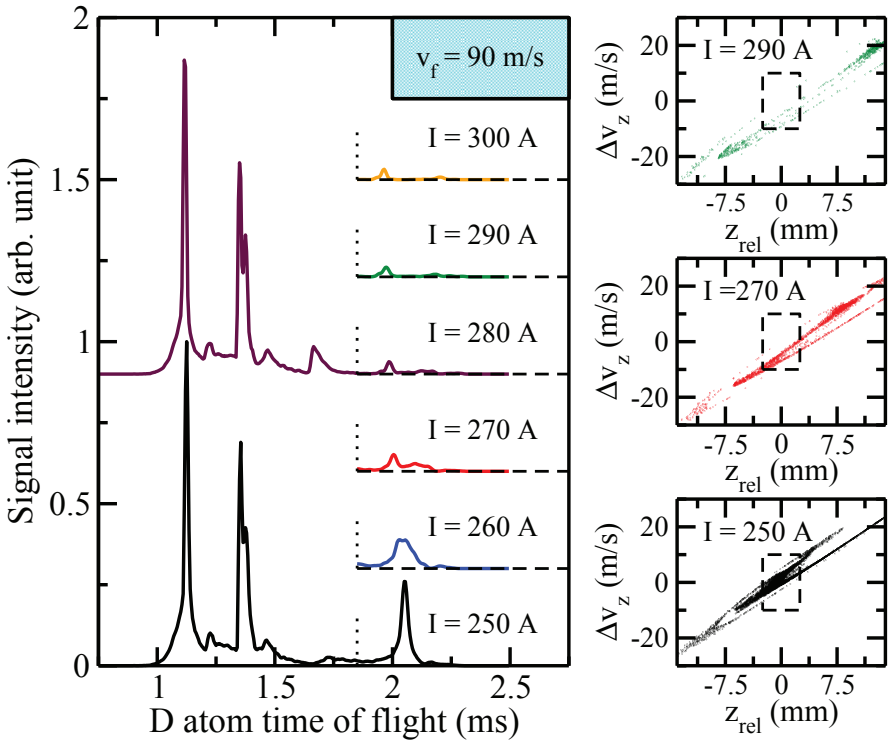

FIG. 6. Simulations of the deceleration of deuterium atoms with identical initial phase-space distributions to a final velocity of 90 m/s, using the constant-energy-removal operation mode of a 24-stage Zeeman decelerator. The deceleration pulse sequences are generated for different currents indicated above the TOF traces. Right-hand side: Phase-space distribution at the end of the decelerator for currents of 290 A, 270 A and 250 A. The dashed rectangles indicate the areas in longitudinal phase space for which magnetic trapping has been achieved.

the constant-energy-removal and constant-nominal-phase-angle operation mode of the decelerator, respectively. Overall, the constant-nominal-phase-angle mode of operation appears slightly superior and can be used over a wider range of currents for the reasons given above. The optimal nominal phase angle increases slightly with decreasing velocity because of the total kinetic energy that must be removed increases. Moreover, the density of slow particles decreases with increasing currents, because these can only be used with low phase angles, for which transverse phase instabilities reduce the acceptance. Finally, the range of nominal phase angles between 45° and 55° for optimal operation, which was determined in the previous section, is confirmed.

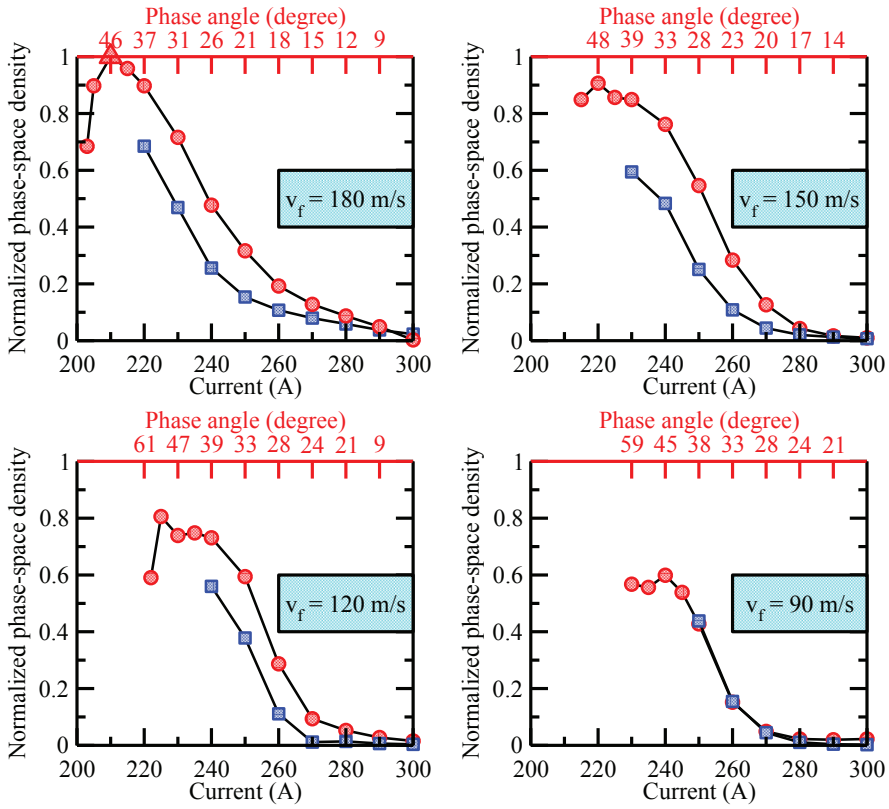

FIG. 7. Phase-space acceptance of a multistage Zeeman decelerator obtained in particle-trajectory simulations carried out for the constant-nominal-phase-angle (circles) and constant-energy-removal (squares) operation modes. The acceptances are determined in a given volume around the synchronous particle (5^3 mm^3 $\times$ 20^3 m^3/s^3 $\cdot$ $m_{\rm D}^3$) at the end of the decelerator and have been normalized to the maximal acceptance highlighted by the red triangle. The four panels display the results obtained for four different final velocities between 90 m/s and 180 m/s.

B. Experimental results and comparison with simulations

To verify the overall conclusions drawn from the simulations, experiments were performed using our multistage Zeeman decelerator. The measurements were carried out for both operational modes discussed in the previous subsection, and we present here the results obtained for magnetic-field pulse sequences designed to decelerate deuterium atoms from an initial velocity of 475 m/s to a final velocity of 150 m/s.

The experimental results are presented in Fig. 8 and Fig. 9 for the constant-nominal-phase-angle and the constant-energy-removal mode of operation of the Zeeman decelerator, respectively. In each figure, the results of the corresponding particle-trajectory simulations

are depicted on the right-hand side for comparison. All simulations were performed with a unique set of parameters (initial phase-space distributions, solenoid characteristics, and experimental geometry) already established and discussed in Ref. [28]. The intensity scale of the simulated traces are identical. To compensate for day-to-day variations of the signal strength, the intensity scale of the experimental traces was adjusted so that all time-of-flight spectra had the same intensity for the first strong peak at 1.2 ms corresponding to the atoms that are guided through the decelerator. This scaling procedure is justified by the insensitivity of this peak to the different pulse sequences predicted by the simulations discussed in the previous section.

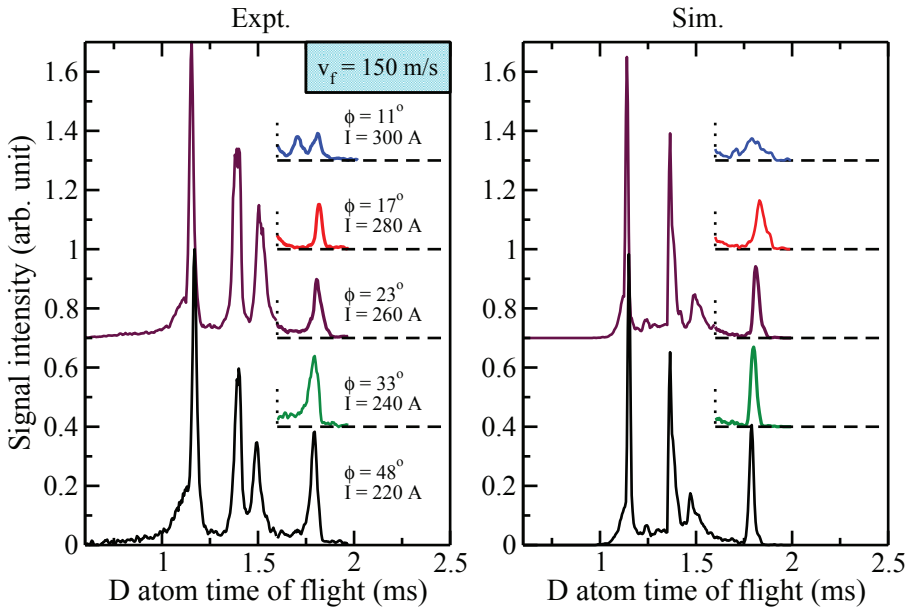

FIG. 8. Experimental traces (left panel) and their corresponding simulations (right panel) for the deceleration of deuterium atoms from an initial velocity of 475 m/s to 150 m/s in a Zeeman decelerator operated in the constant-nominal-phase-angle mode. The TOF profiles are displayed in order of increasing values of the phase angle from top to bottom.

The overall agreement between experimental and calculated TOF traces is good. The main difference concerns the intensity of the third peak at 1.5 ms corresponding to guided atoms, the intensity of which is underestimated by the calculations. The general trends of the intensity of the decelerated peak are nicely reproduced by the calculations so that the general conclusions drawn in subsection III A are validated. In particular, the experimental results confirm that (i) the constant-nominal-phase-angle and constant-energy-removal

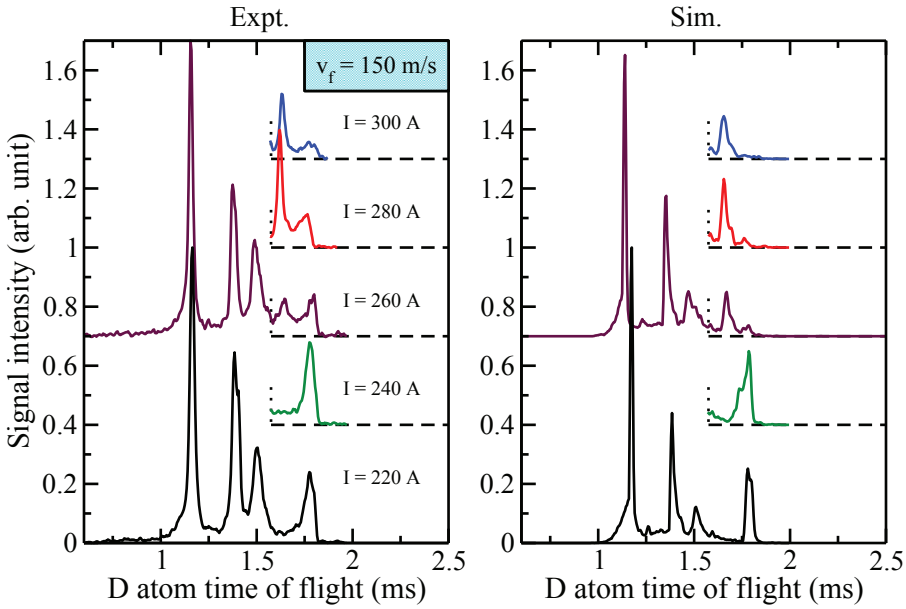

FIG. 9. Experimental (left panel) and simulated (right panel) TOF profiles for the deceleration of deuterium atoms from 475 m/s to 150 m/s in a Zeeman decelerator using the constant-energy-removal mode of operation. The traces are displayed in order of decreasing values of the current from top to bottom.

modes of operation of the decelerator lead to very similar results, the former mode of operation appearing slightly more favorable at the lowest current (220 A, bottom trace Fig. 8); (ii) the decelerated atoms form a bimodal distribution at low phase angles and high currents, an effect that is particularly pronounced in the top trace of Fig. 8 and the top traces of Fig. 9; and (iii) the acceptance of the decelerator improves with increasing phase angles, phase angles in the range around 45° being optimal.

C. Other approaches for the design of efficient deceleration pulse sequences

Because the phase-space density of a given sample cannot be increased by the deceleration process, an optimal deceleration pulse sequence may be regarded as one for which the phase-space acceptance is maximal. Considering only longitudinal effects in the one-dimensional calculations leads to the conclusion that optimal pulse sequences should have as low a phase angle as possible (see Fig. 2 and the left column of Fig. 3). The consideration of the transverse motion and the finite fall times of the magnetic-field pulses, however, leads

to the conclusion that higher equilibrium phase angles are more favorable. The results presented in the previous sections suggest that transverse losses can be avoided in both the constant-nominal-phase-angle and the constant-energy-removal modes of operation of a Zeeman decelerator as long as the phase angles are in the range of $45° - 55°$.

One may nevertheless wonder whether a larger acceptance might not be reached with different magnetic field pulse sequences, i.e., sequences not restricted to constant nominal phase angles or energy removal, such as an operation similar to the $s = 3$ mode in Stark decelerators discussed in subsubsection II B 4. Alternatively, one may use evolutionary strategies to search for deceleration pulse sequences with improved phase-space acceptance as proposed and realized for trap loading at the end of a Stark decelerator [31].

The ability of our particle-trajectory simulation program, demonstrated in the previous subsection (see also Ref. [28]), to faithfully reproduce experimental results for a wide range of operation conditions makes it possible to search for pulse sequences offering improved phase-space acceptance by particle-trajectory simulations. Such sequences, if they exist, may then be tested experimentally. In this last subsection, we present results obtained using evolutionary strategies to optimize the pulse sequences.

An optimization technique based on an evolutionary strategy known as Covariance Matrix Adaptation Evolution Strategy (CMA-ES, see Ref. [33]) was implemented into the particle-trajectory simulation program. The algorithm was employed to (i) maximize the number of particles decelerated to the desired velocity, while (ii) minimizing the velocity and position spread of these particles, by changing the timing and duration of the pulses, with the restrictions of a sequential pulsing of the successive solenoids and a minimal pulse duration of 13 μs dictated by the finite rise and fall times of the current pulses. A (suboptimal) constant-nominal-phase-angle sequence (11°) with a current of 300 A was used to initialize the optimization algorithm, and the operational current was fixed at 300 A, providing maximal flexibility in the choice of phase angles.

The outcome of the optimization for a selected final velocity of 150 m/s is compared with the initial sequence in Fig. 10. The figure presents in its upper panels the simulated and experimental TOF distributions obtained with the initializing sequence (left-hand side) and the optimized sequence (right-hand side). It also shows, in the bottom panel, the magnetic field strength at the position of the synchronous particle during the deceleration process. The nominal phase angle of the individual pulses are also indicated in this panel. The phase

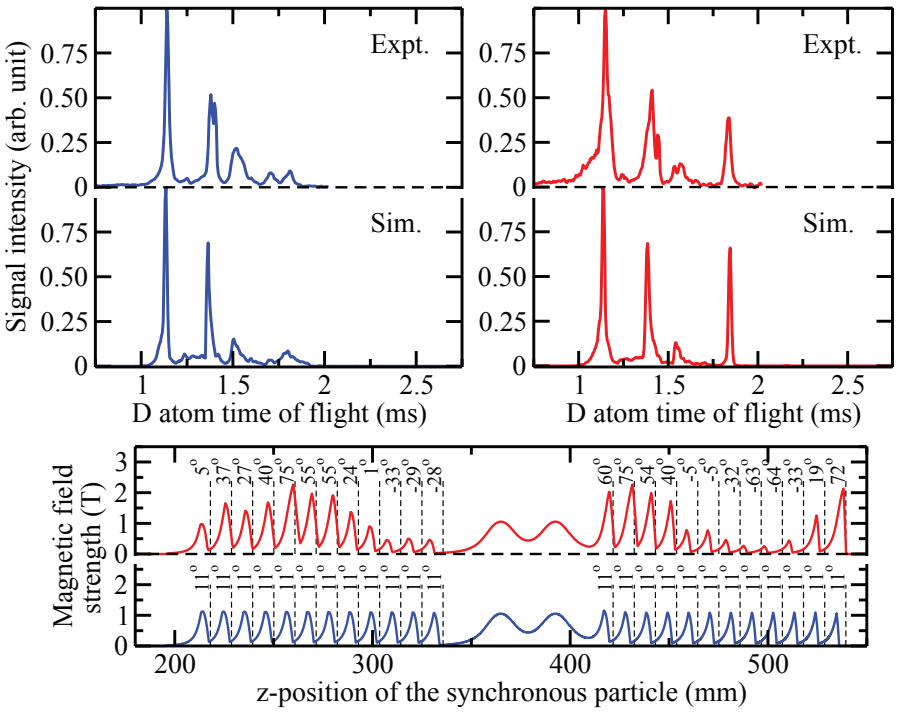

FIG. 10. Upper panels: Experimental and simulated TOF distributions for the deceleration of deuterium atoms from an initial velocity of 475 m/s to a final velocity of 150 m/s in a 24-stage Zeeman decelerator using a constant-nominal-phase-angle mode of operation (left-hand side) and a mode of operation optimized with an evolutionary algorithm (right-hand side). Bottom panel: Magnetic field strength at the position of the synchronous particle for the constant-nominal-phase-angle sequence (bottom) and the optimized sequence (top). The phase angle of each pulse is specified next to the dashed line indicating the center of the active deceleration solenoid. The broad structures near the center of the graph represent the magnetic field of the two focusing solenoids in between the deceleration sections.

angles of the optimized pulse sequence were defined with respect to the particle at the center of the phase-space distribution of the decelerated atoms.

The improved phase-space acceptance of the optimized sequence can be deduced from the figure, the intensity of the decelerated peak being more than one order of magnitude stronger than for the initial constant-nominal-phase-angle sequence. The experimental implementation of the optimized sequence reproduces the strong increase of the intensity of the decelerated atoms. However, this peak is not as sharp as that in the calculation, an effect we attribute to the instrument function and/or the unavoidable slight deviations between

the parameters assumed in the simulations from their actual values.

Comparing the intensity of the peaks corresponding to the decelerated atoms with that of the first strong peak in the TOF distribution suggests that the optimized sequence might be slightly superior to the best sequence obtained with the constant-nominal-phase-angle operation mode (45°, see Fig. 5). Analyzing the results of optimized pulse sequences for a variety of final velocities and operating currents reveals that these sequences are all characterized by a smooth oscillation of phase angles (for example between $-5°$ and $75°$ for the optimized sequence displayed in Fig. 10) providing an optimal balance between transverse focusing and defocusing forces during the deceleration process. It is interesting to point out here that by searching, by trial and error, for optimal pulse sequences by monitoring the intensity of the decelerated peak on the oscilloscope, a pulse sequence was found that has similar characteristic features as the one selected by the evolutionary algorithm [28].

From these results we conclude that, while evolutionary strategies can be used to design deceleration pulse sequences with large phase-space acceptance, constant-nominal-phase-angle pulse sequences with phase angles in the range $45° - 55°$ are close to optimal and are therefore recommended as easily implemented, efficient pulse sequences for multistage Zeeman deceleration. This advantage is expected to be essential in the realization of very long decelerators.

IV. ACKNOWLEDGMENT

We thank M. Andrist, H. Schmutz, J. Agner, and B. Lambillotte for their help in the development of the Zeeman decelerator, and Y. Salathé for useful discussions and for his contributions to the development of the particle-trajectory-simulation program. This work was supported by the Swiss National Science Foundation under project 200020-122128, the ERC advanced grant program (Grant Nr. 228286) and the QSIT initiative of ETH.

[1] R.V. Krems, Phys. Chem. Chem. Phys. **10**, 4079 (2008).

[2] S. Y. T. van de Meerakker, H. L. Bethlem, and G. Meijer, Nature Phys. **4**, 595 (2008).

[3] M. T. Bell and T. P. Softley, Mol. Phys. **107**, 99 (2009).

[4] L. D. Carr, D. DeMille, R. V. Krems, and J. Ye, New J. Phys. **11**, 055049 (2009).

[5] C. G. Parthey, A. Matveev, J. Alnis, R. Pohl, T. Udem, U. D. Jentschura, N. Kolachevsky, and T. W. Hänsch, Phys. Rev. Lett. **104**, 233001 (2010).

[6] I. R. Sims and I. W. M. Smith, Annu. Rev. Phys. Chem. **46**, 109 (1995).

[7] J. J. Gilijamse, S. Hoekstra, S. Y. T. van de Meerakker, G. C. Groenenboom, and G. Meijer, Science **313**, 1617 (2006).

[8] M. R. Tarbutt, H. L. Bethlem, J. J. Hudson, V. L. Ryabov, V. A. Ryzhov, B. E. Sauer, G. Meijer, and E. A. Hinds, Phys. Rev. Lett. **92**, 173002 (2004).

[9] E. Narevicius, A. Libson, C. G. Parthey, I. Chavez, J. Narevicius, U. Even, and M. G. Raizen, Phys. Rev. Lett. **100**, 093003 (2008).

[10] H. L. Bethlem, G. Berden, and G. Meijer, Phys. Rev. Lett. **83**, 1558 (1999).

[11] H. L. Bethlem, G. Berden, F. M. H. Crompvoets, R. T. Jongma, A. J. A. van Roij, and G. Meijer, Nature (London) **406**, 491 (2000).

[12] Y. Yamakita, S. R. Procter, A. L. Goodgame, T. P. Softley and F. Merkt, J. Chem. Phys. 121, 1419 (2004).

[13] E. Vliegen and F. Merkt, J. Phys. B: At. Mol. Opt. Phys. **38** 1623 (2005).

[14] S. D. Hogan and F. Merkt, Phys. Rev. Lett. **100**, 043001 (2008).

[15] S. D. Hogan, Ch. Seiler and F. Merkt, Phys. Rev. Lett. **103**, 123001 (2009).

[16] N. Vanhaecke, U. Meier, M. Andrist, B. H. Meier, and F. Merkt, Phys. Rev. A **75**, 031402(R) (2007).

[17] S. D. Hogan, D. Sprecher, M. Andrist, N. Vanhaecke, and F. Merkt, Phys. Rev. A **76**, 023412 (2007).

[18] E. Narevicius, C. G. Parthey, A. Libson, J. Narevicius, I. Chavez, U. Even, and M. G. Raizen, New. J. Phys. **9**, 358 (2007).

[19] S. D. Hogan, A. W. Wiederkehr, H. Schmutz, and F. Merkt, Phys. Rev. Lett. **101**, 143001 (2008).

[20] V. J. Veksler, J. Phys. (Moscow) **9**, 153 (1945).

[21] E. M. McMillan, Phys. Rev. **68**, 143 (1945).

[22] H. L. Bethlem, G. Berden, A. J. A. van Roij, F. M. H. Crompvoets, and G. Meijer, Phys. Rev. Lett. **84**, 5744 (2000).

[23] S. Y. T. van de Meerakker, N. Vanhaecke, H. L. Bethlem, and G. Meijer, Phys. Rev. A **73**, 023401 (2006).

[24] S. Y. T. van de Meerakker, N. Vanhaecke, H. L. Bethlem, and G. Meijer, Phys. Rev. A **71**, 053409 (2005).

[25] L. Scharfenberg, H. Haak, G. Meijer, and S. Y. T. van de Meerakker, Phys. Rev. A **79**, 023410 (2009).

[26] S. A. Meek, H. L. Bethlem, H. Conrad, and G. Meijer, Phys. Rev. Lett. **100**, 153003 (2008).

[27] A. Osterwalder, S. A. Meek, G. Hammer, H. Haak, and G. Meijer, Phys. Rev. A **81**, 051401(R) (2010).

[28] A. W. Wiederkehr, S. D. Hogan, B. Lambillotte, M. Andrist, H. Schmutz, J. Agner, Y. Salathé, and F. Merkt, Phys. Rev. A **81**, 021402(R) (2010).

[29] H. L. Bethlem, F. M. H. Crompvoets, R. T. Jongma, S. Y. T. van de Meerakker, and G. Meijer, Phys. Rev. A **65**, 053416 (2002).

[30] B. Friedrich, Eur. Phys. J. D **31**, 313 (2004).

[31] J. J. Gilijamse, J. Küpper, S. Hoekstra, N. Vanhaecke, S. Y. T. van de Meerakker, and G. Meijer, Phys. Rev. A **73**, 063410 (2006).

[32] S. D. Hogan, A. W. Wiederkehr, M. Andrist, H. Schmutz, and F. Merkt, J. Phys. B **41**, 081005 (2008).

[33] N. Hansen, *Studies in Fuzziness and Soft Computing*, edited by J.A. Lozano, P. Larrañaga, I. Inza and E. Bengoetxea (Springer, 2006), Vol. 192, p 75.